Large-eddy simulation of flow around an airfoil on a structured mesh

By Hans-Jakob Kaltenbach AND Haecheon Choi

1. Motivation and objectives

The diversity of flow characteristics encountered in a flow over an airfoil near maximum lift taxes the presently available statistical turbulence models. This work describes our first attempt to apply the technique of large-eddy simulation to a flow of aeronautical interest. The challenge for this simulation comes from the high Reynolds number of the flow as well as the variety of flow regimes encountered, including a thin laminar boundary layer at the nose, transition, boundary layer growth under adverse pressure gradient, incipient separation near the trailing edge, and merging of two shear layers at the trailing edge.

The flow configuration chosen is a NACA 4412 airfoil near maximum lift. The corresponding angle of attack was determined independently by Wadcock (1987) and Hastings & Williams (1984, 1987) to be close to 12°. The simulation matches the chord Reynolds number $U_\infty c/\nu = 1.64 \times 10^6$ of Wadcock's experiment.

2. Accomplishments

2.1 Numerical method and SGS model

The numerical method for solving the unsteady, incompressible Navier-Stokes equations is described in Choi *et al.* (1993). Second-order spatial central differences on a staggered mesh are combined with a semi-implicit time integration scheme. Formulation of the problem in terms of contravariant velocity components, weighted with the Jacobian, in conjunction with the staggered variable configuration leads to discretized equations that can be solved with the classical splitting approach. The resulting pressure Poisson equation is solved using FFT for the spanwise (periodic) direction and iterative methods for the remaining two-dimensional problems. The computational cost is about equally distributed between computation of the right-hand side and solving the Poisson equation at every substep of a third order Runge Kutta time integration.

The implementation of the dynamic subgrid-scale model (Germano *et al.* 1991) with least-square contraction (Lilly 1992) uses the spanwise homogeneity of the flow to obtain a model coefficient that is a function of streamwise and wall-normal coordinate only. We found that the dynamic procedure occasionally renders unrealistic negative coefficients in regions where the flow is laminar such as at the nose or in the potential flow region. In these regions, the negative values are the result of the dynamic model becoming ill-conditioned and have no physical significance. In the present simulations we prevented any form of backscatter by constraining the model coefficient to be always positive.

x/c	δ_{99}/c	$\Delta x/c$	Δx^+	Δz^+	$\Delta x/\Delta z$	δ_{99}/L_z
0.1	0.004	0.0031	405	137	2.96	0.08
0.2	0.006	0.0033	378	118	3.2	0.12
0.4	0.016	0.0033	274	86	3.2	0.32
0.6	0.030	0.0050	235	49	4.8	0.6
0.8	0.060	0.0088	110	13	8.5	1.2

Table 1. Spacing along upper surface of airfoil. The last two columns show cell aspect ratio and ratio of boundary layer thickness to domain width for case A.

On the present mesh, the CFL limit of 1.5 results in an average timestep of $2 \times 10^{-4} c/U_\infty$. About 80 CPU-seconds on a Cray-C90 are needed to advance the solution over one timestep on a mesh of $638 \times 79 \times 48 = 2.4 \times 10^6$ cells. Therefore, simulation of one time unit c/U_∞ requires 90 CPU-hours. In order to obtain smooth statistics the results have to be averaged over several time units.

2.2 Computational domain and mesh layout

The computational domain is a C-mesh with the outer boundary about three chord lengths away from the surface. At the outer boundary we specify the freestream velocity U_∞. As a consequence, the vertical velocity component (in a coordinate system aligned with the chord at 0° angle of attack) will be zero at the outer boundary. Therefore, the chosen configuration resembles more the flow around an airfoil inside of a wind tunnel with parallel walls than an airfoil in free air. Jansen (1995) has shown that, even with the walls located much closer, the presence of wind tunnel walls mainly affects the flow in the nose region by increasing the suction peak. The pressure distribution in the rear part and the size of the backflow zone, however, are only weakly dependent on whether the wind tunnel walls are included or not. A no-slip condition is enforced at the airfoil surface, and we use a convective (radiative) boundary condition at the outflow plane.

Results from two simulations will be presented. The two cases differ only with respect to the spanwise domain width which is $0.05c$ in case A and $0.025c$ in case B. The spanwise spacing Δz is the same with 48 cells in case A and 24 cells in case B, respectively. Main criterion for the choice of the spanwise domain size is the ratio of boundary layer thickness to domain width, which is tabulated in Table 1. As a consequence of the rapid growth of the boundary layer thickness on the suction side, this ratio, which is initially sufficiently small to capture several structures in the spanwise direction, exceeds one near the trailing edge. It is likely that the development of flow structures in the outer part of the boundary layer will be affected by the limited domain size. Comparison of cases A and B gives insight in the sensitivity of the simulation with respect to this parameter.

The design of an adequate mesh involves several aspects. The most energetic eddies of the boundary layer have to be resolved. More or less general criteria have been developed for the mesh spacing in the case of wall bounded shear flows under zero pressure gradient. However, these criteria depend on the numerical method employed (Lund *et al.*, 1995). Cabot (1994) found that for LES of turbulent channel flow based on second-order finite differences a spacing of $\Delta x^+ = 60$ and

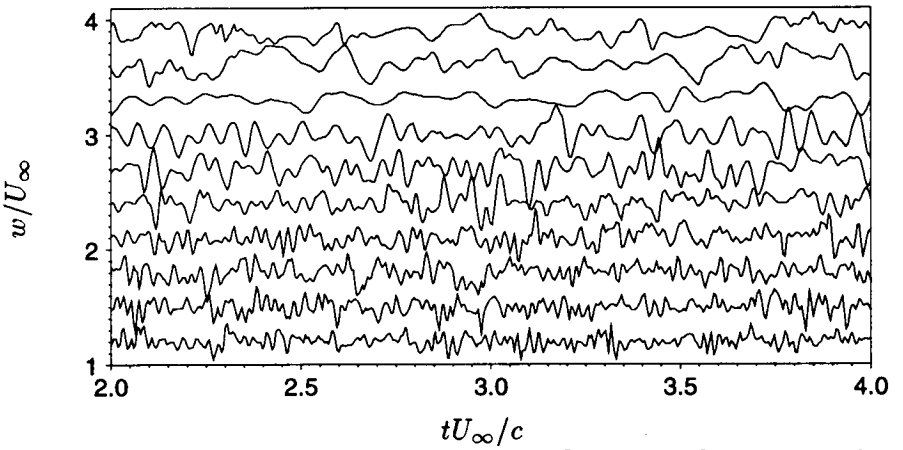

FIGURE 1. Time series of spanwise velocity fluctuation between stations $x/c = 0.24$ (bottom) and $x/c = 0.98$ (top) at about 5% of the local boundary layer height. Individual curves are separated by a vertical offset of 0.3 with the corresponding zero-lines located at 1.2, 1.5, ... 3.9.

$\Delta z^+ = 15 - 20$ is needed to adequately resolve the near wall structures.

Little is known about the minimum spacing requirements for boundary layers which are close to separation. The mesh size in terms of wall units probably becomes less relevant in this case. About half of the 640 streamwise points were distributed over the upper surface, which guaranteed that the streamwise spacing was between 1/3 and 1/5 of the local boundary layer thickness for most of the upper surface, see Table 1. The streamwise spacing varies considerably along the surface due to the boundary layer growth. Near the trailing edge, the grid was refined in x in order to resolve the merging of the two shear layers. No attempt was made to resolve the turbulence on the lower side of the airfoil. Spacings in terms of wall units based on the local skin friction as given in Wadcock's experiment are given in Table 1. It is evident that the spacing in the present simulation is considerably coarser than what has been found to be necessary for channel flow simulations. However, as the boundary layer develops along the surface, the resolution criteria become less restrictive so that the flow in the rear part is much better resolved than in the front section.

In the wall-normal direction we used a hyperbolic mesh generator (Chan, 1993) to distribute 79 layers of cells. The first line away from the wall was at about $y^+ = 1$, and over most of the surface there were between 20 and 30 points inside the boundary layer.

2.3 Difficulties arising from the high Reynolds number

Centered difference schemes suffer from the emergence of grid-to-grid oscillations (2-Δ-waves, wiggles) when used for high Reynolds number simulations. Usually, the viscosity provided by the subgrid-scale model is sufficient to dampen these grid-to-grid oscillations. Several sources for 2-Δ-waves have been identified in the past (Gresho, 1981). They include high cell Peclet numbers in conjunction with large

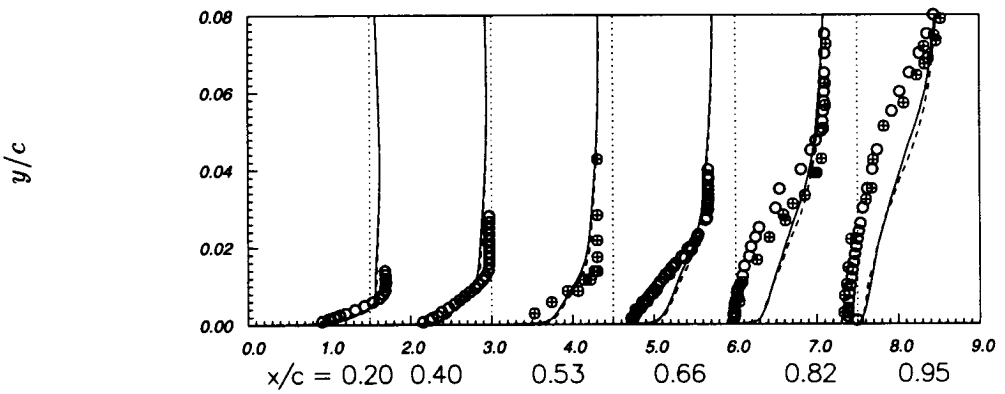

FIGURE 2. Mean velocity profiles, normalized by U_∞, along upper surface. Symbols: case A ——— , B - - - - , measurements by Hastings o and Wadcock + .

streamwise gradients of the advected variable. This situation is typically encountered near the nose and the trailing edge of the airfoil. Other sources are the outflow boundary (an artificial boundary layer is generated in the streamwise direction) and mesh stretching. As shown by Cain & Bush (1994), waves propagating into an increasingly coarse (fine) mesh are amplified (dampened) in a centered scheme. In our simulation we find that strong 2-Δ-waves appear near the nose and near the trailing edge. The wiggles appear almost exclusively in the streamwise coordinate direction. Part of these waves travel with different phase speed and cancellation occurs. However, other parts are steady and accumulate in time. These standing waves contaminate the potential flow region after long integration times. It is difficult to assess to what degree the solution is contaminated by the presence of 2-Δ-waves. On a staggered mesh, velocity components are averaged in order to obtain fluxes at cell faces. This averaging on a scale of the mesh cell can sometimes completely hide the 2-Δ-wave. For example, the convective term $\partial(uu)/\partial x$ in the streamwise momentum balance is evaluated as

$$\frac{1}{\Delta x}\left[\left(\frac{u_{i+1}+u_i}{2}\right)^2-\left(\frac{u_i+u_{i-1}}{2}\right)^2\right] .$$

The finite difference expression renders the same value independently whether an oscillatory part in the i-direction $\tilde{u_i} = (-1)^i u_a$ with zero mean and arbitrary amplitude u_a is added or not. Similarly, if a 2-Δ-wave in the i-direction is present in the v velocity component, it will not appear in the discrete approximation for $\partial(uv)/\partial y$. However, it will contaminate the term $\partial(uv)/\partial x$. Time averaged fields of velocity components show 2-Δ-waves in the potential flow region, but the pressure field is virtually free of wiggles. This indicates that the presence of 2-Δ-waves in the potential flow region may be tolerated to a certain degree since wiggle free streamlines in accordance with the pressure field can be reconstructed.

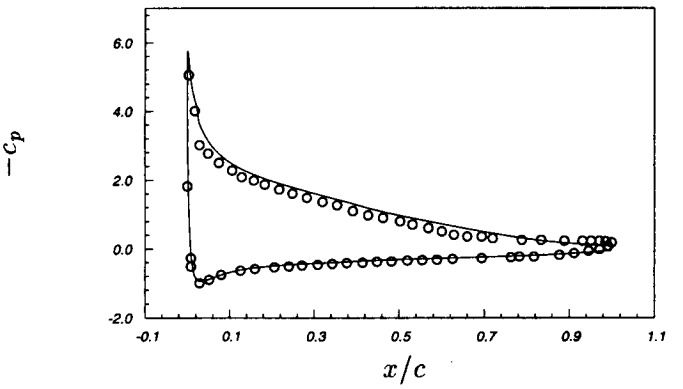

FIGURE 3. Pressure distribution around the airfoil. Symbols: LES ——— , Wadcock o .

The strongest effect of 2-Δ-waves comes from the associated limitations for the computational timestep. Large amplitude wiggles in the wall normal velocity component in conjunction with rather fine wallnormal spacing cause high CFL numbers near the nose. The resulting timestep limitations are so severe that the simulation can not be carried out at an affordable cost. We therefore resorted to an *ad hoc* modification of the numerical scheme. In a small region near the nose (less than 2% of the chord) we applied a 1:2:1-filter in the streamwise and spanwise direction which efficiently eliminates all 2-Δ-waves. Filtering is equivalent to adding a direction dependent diffusion term to the equations. Justification for this procedure comes from the fact that the flow near the nose is laminar and filtering on a scale of the grid cell does not affect the flow physics. Additionally, the boundary layer in the experiments was tripped at a location around $x/c = 0.02$, thereby fixing the region of laminar-turbulent transition. We find that the flow spontaneously transitions as soon as the filter ends. In this sense, we control the location of transition by setting the streamwise extent of the region where the solution is filtered. The filter extended about 40 layers away from the wall and faded to zero over another 15 layers. Unfortunately, this procedure changes the potential flow significantly. Because the mesh cells are rather large in the outer part of the domain, filtering on the grid scale is no longer negligible on the scale where the potential flow changes near the nose. Future simulations can easily avoid this problem by limiting the filter to the vicinity of the surface, i.e. it should end near the boundary layer edge. No attempt was made to dampen 2-Δ-waves in the trailing edge region where the flow is fully turbulent. Any filtering there would probably affect the flow physics.

2.4 Simulation results and discussion

Figure 1 shows time series of the spanwise velocity fluctuation w recorded at several stations along the upper surface of the airfoil. We observe a shift in the frequency which corresponds to the most energetic motions towards lower values as the recording station moves closer to the trailing edge. This is consistent with the

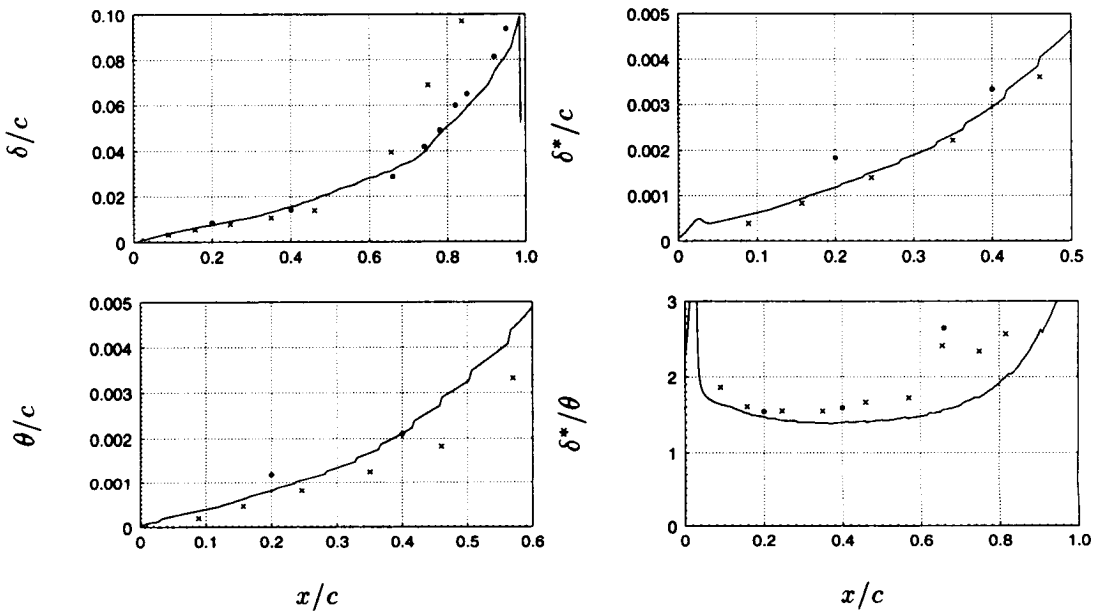

FIGURE 4. Boundary layer thickness δ, displacement thickness δ^*, momentum thickness θ and shape factor $H = \delta^*/\theta$ along the upper surface of the airfoil. Symbols: —— LES, • Hastings, × Wadcock.

increase of an inertial timescale (ratio of the boundary layer thickness to the edge velocity) as the boundary layer grows under the influence of the adverse pressure gradient. It becomes evident that the solution has to be sampled over several time units c/U_∞ in order to obtain representative turbulence statistics for the rear part of the airfoil.

Statistics were obtained by averaging the instantaneous flow fields in the spanwise homogeneous direction and in time over more than $2c/U_\infty$. Profiles of the mean velocity in a surface normal coordinate system are shown in Fig. 2. At the first two stations, the edge velocity is about 12% smaller than measured by Hastings. As mentioned earlier, this is a side effect from the filter which was applied in the nose region in order to eliminate 2-Δ-waves. Since filtering was limited to a region close to the surface, simulated and measured mean flow agree much better for distances greater than $y/c = 0.06$. Although a better match between simulated and measured edge velocity is desirable (and can easily be obtained by further reducing the distance from the surface over which the filter is applied), we don't expect turbulence statistics to be significantly affected. One reason is the observation that the simulated adverse pressure gradient matches the measured one over most of the upper surface, see Fig. 3. Filtering affects mainly the magnitude of the suction peak and is partially responsible for the offset in the simulated pressure distribution. Additionally, since wind tunnel walls were not properly considered in this simulation, the pressure distribution near the nose will deviate from the measured one, see Jansen (1995). The goal of the present study is to predict the boundary layer growth and

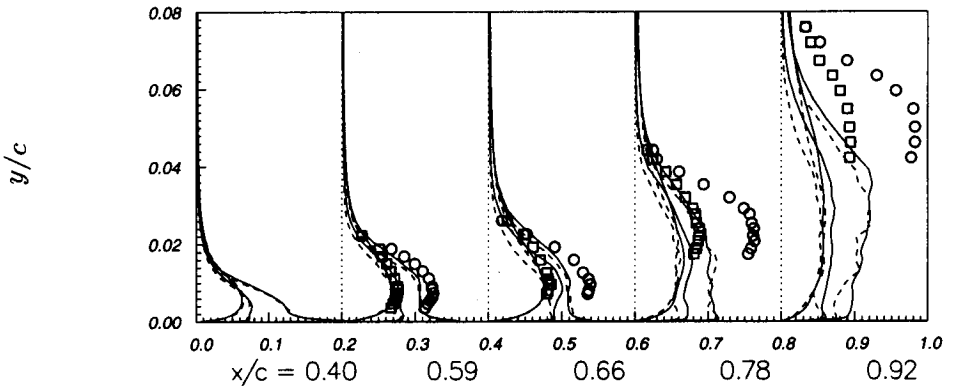

FIGURE 5. RMS of velocity fluctuations u', v' and w', normalized with U_∞. Symbols: case A ——— , B - - - - , u' ○ and v' □ from Hastings. In terms of relative magnitude, the three curves for each simulation are v', w', and u' respectively.

the amount of separation near the trailing edge. Accurate prediction of the suction peak is of secondary interest.

Displacement and momentum thickness from the simulation lie in between the measurements of Hastings & Williams (1984) and Wadcock (1987) upstream of $x/c = 0.4$, see Fig. 4. The experimental values differ by up to 40% as a result of differences in boundary layer tripping and Reynolds number. However, the measured shape factor $H \approx 1.55$ is similar in both experiments in the region $x/c = 0.2...0.4$. Contrary to the experiment, H drops gradually in the simulation in the region $x/c = 0.2...0.4$ and reaches values as low as 1.4.

Since both experiments measure similar boundary layer growth and flow retardation near the trailing edge, the flow development does not seem to be very sensitive with respect to the exact values of δ^* and θ of the turbulent boundary that develops behind the transition strip. Although the thickness of the simulated boundary layer is close to the measured ones in the front part of the airfoil, the underprediction of the shape factor in the simulation and the initially opposite trend (decline as opposed to a growth) indicates insufficiencies in the simulated boundary layer for a considerable part of the upper surface. This is not surprising since the resolution is so coarse that the near wall structures can hardly be resolved properly. Examination of instantaneous flow fields close to the surface reveals a very streaky structure with typical spacings in the order of a few mesh cells. Similarly, spanwise two point correlations show a zero-crossing within 2-3 spanwise grid points for all near-wall locations upstream of $x/c = 0.5$, see Fig. 6. This indicates that the simulation has marginal resolution near the wall. Further evidence comes from the comparison of the present case with an earlier simulation which was a factor of 2 coarser in the streamwise direction and a factor of 1.5 coarser in the spanwise direction. The flow

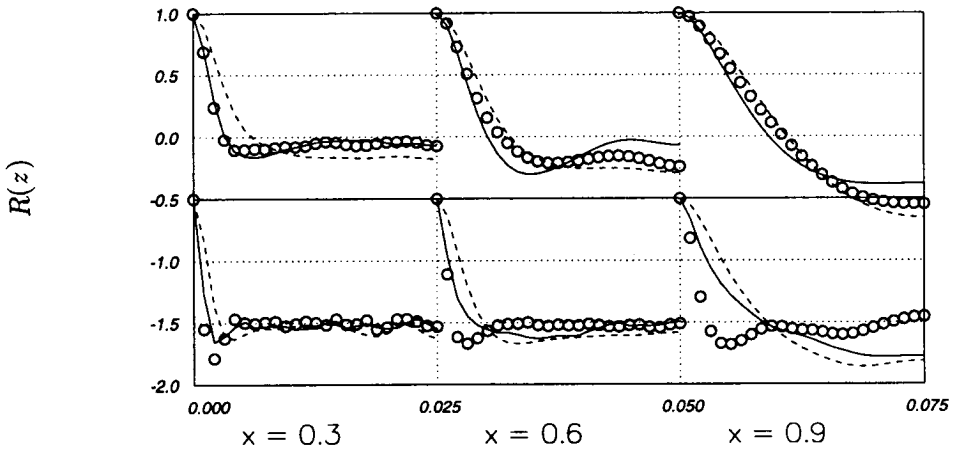

FIGURE 6. Spanwise two-point correlations R_{uu} (——), R_{vv} (o) and R_{ww} (----) versus distance z/c for three stations along the upper surface. Bottom figures correspond to the near wall region, top figures to $y/\delta \approx 0.3$. The y coordinate of the lower figures is shifted, i.e. $y = -1.5$ corresponds to a zero correlation.

retardation and the boundary layer growth was significantly improved on the finer mesh. Therefore, further grid refinement and, subsequently, a better prediction of the boundary layer in the front region might lead to better agreement between simulation and measurements over the entire airfoil.

The shear stress provided by the SGS model is an indicator for the role of the SGS model. The maximum contribution is about 15% of the resolved stress $\overline{uv}$ and is found in the front part of the airfoil where the resolution is coarse. Near the trailing edge, the SGS stress is negligible compared to the resolved Reynolds shear stress. The ratio of SGS eddy viscosity to molecular viscosity is about 20, which emphasizes the important role of the model for the kinetic energy budget.

RMS values of the velocity fluctuations are shown in Fig. 5. Agreement between simulation and experiment is reasonable in the middle section of the airfoil. In a characteristic manner for an adverse pressure gradient boundary layer, the location of maximum rms values (and Reynolds shear stress) moves towards the outer part of the boundary layer. Also, the anisotropy of the fluctuations in the outer part of the boundary layer is greatly reduced. Substantial differences between simulation and experiment are indicated by the large discrepancy in simulated and measured rms values (and shear stress) near the trailing edge. It is unclear whether this mismatch is a local effect or rather a result of differences in (spatial) flow history between experiment and simulation.

Results from cases A and B, which only differ with respect to the spanwise domain size, are surprisingly similar. Two-point correlations from the outer part of the boundary layer of case A do not drop to zero within half the spanwise width for locations downstream of $x/c = 0.6$, see Fig. 6. This means that the large scales

of motion are affected by the presence of artificial periodic boundaries. Since the limitations are much more severe in case B as compared to A, one would expect that both cases deviate in the rear part. Presently, it is not clear why the simulation is rather insensitive with regard to the domain width. Kaltenbach (1994) made a similar observation for a flow in a diffuser where the aspect ratio of the outlet duct was smaller than 0.5. Doubling the aspect ratio had only a small effect on the flow evolution. The cost for case B is about half that of case A. Further studies on the effect of grid refinement would be much cheaper if the domain width of case B turns out to be sufficient.

3. Conclusions and future goals

Wall resolving LES of flow around an airfoil has been demonstrated to be feasible with present computers and standard numerical schemes for LES. Qualitatively, the simulation captures typical features of separating flows such as boundary layer retardation and drastic increase in Reynolds stresses. This demonstrates the capability of the LES concept to deal with flows in complex configurations of immediate technical interest. However, the resolution provided was probably too coarse to adequately simulate the boundary layer in the first half of the airfoil. Although the resolution might have been adequate for the rear part, the overall agreement with measurements with respect to prediction of backflow is not satisfactory. History effects might play a role, and further studies should attempt to match better the integral boundary layer parameters of the experiment at an early station. Because of conservation properties, the use of centered difference schemes is very desirable in the context of LES. However, the emergence of 2-Δ-waves is a serious problem for the present high Reynolds number flow and needs further consideration, for example, usage of explicit filters as explored by Lund & Kaltenbach in this volume. Comparison of two cases with different domain width did not show significant sensitivity with respect to this parameter in the range considered. Future simulations should consider the effect of wind tunnel (top and bottom) walls by a corresponding modification of domain size and boundary conditions.

REFERENCES

CABOT, W. 1994 Local dynamic subgrid-scale models in channel flow. In *Annual Research Briefs 1994,* Center for Turbulence Research, Stanford Univ./NASA Ames Research Center, 143-159.

CAIN, A. B. & BUSH, R. H. 1994 Numerical wave propagation analysis for stretched grids.*AIAA-94-0172*, 32nd Aerospace sciences meeting, Jan. 10-13, 1994, Reno, NV.

CHAN, W. M. 1993 User's Manual for the HYPGEN hyperbolic grid generator. *NASA Technical Memorandum 108791.*

CHOI, H., MOIN, P. & KIM, J. 1993 Direct numerical simulation of turbulent flow over riblets . *J. Fluid Mech.* **255,** 503-539.

GERMANO, M., PIOMELLI, U., MOIN, P. & CABOT, W. H. 1991 A dynamic subgrid-scale eddy viscosity model. *Phys. Fluids A.* **3,** 1760-1765.

GRESHO, P. M. & LEE, R. L. 1981 Don't suppress wiggles - they're telling you something. *Computers & Fluids.* **9,** 223-253.

HASTINGS, R. C. & WILLIAMS, B. R. 1984 Studies of the flow field near an NACA 4412 aerofoil at nearly maximum lift. *Royal Aircraft Establishment, Technical Memorandum Aero 2026.*

HASTINGS, R. C. & WILLIAMS, B. R. 1987 Studies of the flow field near an NACA 4412 aerofoil at nearly maximum lift. *Aeronautical Journal.* **91,** 29-44.

JANSEN, K. 1995 Preliminary large-eddy simulations of flow around a NACA 4412 airfoil using unstructured grids. *Article in this volume.*

KALTENBACH, H.-J. 1994 Large eddy simulation of flow through a plane, asymmetric diffuser. In *Annual Research Briefs 1994,* Center for Turbulence Research, Stanford Univ./NASA Ames Research Center, 175-184.

LILLY, D. K. 1992 A proposed modification of the Germano subgrid scale closure method. *Phys. Fluids A.* **3,** 2746-2757.

LUND, T. S., KALTENBACH, H.-J. & AKSELVOLL, K. 1995 On the behavior of centered finite difference schemes for large eddy simulation. In *Proceedings of the sixth International Symposium on Computational Fluid Dynamics,* Lake Tahoe, NV, 4-8 September, 1995.

WADCOCK, A. J. 1987 Investigation of low-speed turbulent separated flow around airfoils. *NASA contractor report 177450.*